Proceedings of the ASME 2016 14th International Conference on Nanochannels, Microchannels, and Minichannels
ICNMM2016
July 10-14, 2016, Washington, DC, USA

ICNMM2016-7959

EXPERIMENTAL STUDY ON LOCAL SUBCOOLED FLOW BOILING HEAT TRANSFER IN A VERTICAL MINI-GAP CHANNEL

Jun-ye Li[1,2]
1. Department of Energy Engineering, Zhejiang University
2. Department of Energy Engineering, Collaborative Innovation Center of Advanced Aero-Engine, Zhejiang University
Hangzhou, Zhejiang, China

Zhao-zan Feng[3]
3. CRRC Zhuzhou Institute Co., Ltd.
Zhuzhou, Hunan, China

Carolyn Coyle[4], **Thomas J McKrell**[4], **Jacopo Buongiorno**[4]
4. Department of Nuclear Science and Engineering, Massachusetts Institute of Technology,
Cambridge, Massachusetts 02139, USA

Kan Zhou[1,2]
1. Department of Energy Engineering, Zhejiang University
2. Department of Energy Engineering, Collaborative Innovation Center of Advanced Aero-Engine, Zhejiang University
Hangzhou, Zhejiang, China

Wei Li[1*]
1. Department of Energy Engineering, Zhejiang University
Hangzhou, Zhejiang, China
Weili96@zju.edu.cn

ABSTRACT

An experimental study of subcooled flow boiling in a high-aspect-ratio, one-sided heating rectangular mini-gap channel was conducted using deionized water. The local heat transfer coefficient, onset of nucleate boiling, and flow pattern of subcooled boiling were investigated. The influence of heat flux and mass flux were studied with the aid of a high-speed camera. The results show that the flow pattern was mainly isolated bubbly flow when the narrow microchannel was placed vertically. The bubbles generated at lower mass fluxes were larger and did not easily depart, forming elongated bubbly flow and flowing upstream. The thin film evaporation mechanism dominated the entire test section due to the elongated bubbles and transient local dryout as well as rewet. The local heat transfer coefficient near the exit of the test section was larger.

INTRODUCTION

Highly efficient heat-dissipation system is of great importance to the operation, duration, and performance of high power components such as IGBT chips. The conventional air cooled and water cooled heat exchangers are unable to meet the need of high heat-flux dissipation density due to the increased power consumption and decreased size of these devices[1]. Tuckerman and Pease found that the microchannel heat sink was a very promising solution for highly efficient heat dissipation in 1981[2]. Higher heat transfer coefficient, better uniformity of temperature distribution, and lower mass flux as well as lower pump power needed can be realized by utilizing phase change in the evaporators. Meanwhile, there is a variety of complicated problems in the microchannel, such as the instability of flow boiling, which imposes limitations on the application of two phase heat transfer in microchannels. A comprehensive review about the research progress of the

microchannel in recent two decades was given by Kandlikar[3]. He concluded that there is no distinct difference between the single-phase heat transfer in the microchannel and that in the classic macroscale channel. The divergences in the literature mainly existed in the two phase flow boiling. The bubbles generated by liquid boiling are confined in microchannels when the channel size is too small, which gives distinctly difference in the flow patterns, heat transfer, pressure drop, instability and critical heat flux compared with the macroscale channels[4,5].

There have been many experimental studies for the flow boiling in parallel microchannels, whose primary drawbacks are the flow instability and relatively high pressure drop. The bubbles generated in the narrow microchannel can expand in both axial and widthwise direction in the growth period compared to the parallel microchannels, which greatly improves the flow instability and reduces pressure drop penalties[6-8]. However, the narrow microchannel has disadvantages such as relatively small heat transfer area and heat transfer coefficient. Surface modification techniques are adopted to improve the heat transfer coefficient [9, 10].

In the present study experimental measurements and visualizations were carried out for the ONB (Onset of Nucleate Boiling) and local heat transfer coefficient of subcooled flow boiling in the narrow microchannel with deionized water as the working fluid.

EXPERIMENTAL METHOD

Experimental apparatus

Figure 1 shows the schematic of the flow boiling experimental setup. Before the boiling test, deionized water was fully degassed by boiling. The deionized and degassed water flowed through the gear pump, filters, mass flow meter, high temperature water bath, electrical heating section and the test section. Finally the water flowed into the plate heat exchanger where it was cooled and flowed back to the storage tank. It is noteworthy that the test section was immersed in a home-built thermostat air bath to minimize the heat loss to about 3%.

The inlet and outlet fluid temperatures were measured by the 0.3 mm T-type thermocouple and 1 mm outer-diameter K-type thermocouple, respectively. The wall temperature sensors of the test section were fabricated by soldering 0.254 mm T-type thermocouples. All thermocouples were calibrated using a constant temperature water bath. The gauge pressure at the entrance of the test section was measured by a pressure transmitter and the differential pressure in the test section was measured by a differential pressure transmitter. All the relevant parameters were recorded by Agilent 34970A at 5 second intervals.

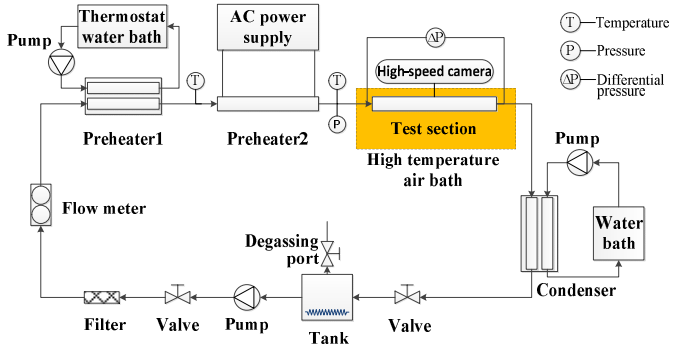

Figure 1. Schematic of setup for flow boiling in micro/mini-channels

The narrow microchannel test section is the core of the experimental setup. It is composed of four main components: (1) top cover made of PSU(Polysulfone), above which a microgroove with 80mm length and 0.52 × 5.01 mm^2 section area is machined, as shown in Figure 2a, (2) bottom base made of PSU, with the entrance and exit mixing columns, guide holes of the pressure, and the groove of 15 × 30 × 8 mm^3, (3) PEEK(Polyetheretherketone) holder integrated with temperature sensors and copper electrodes, (4) flat silicon heater. The heater mainly consists of a 0.02 mm-thick Ruthenium oxide serpentine heater, a 0.4 mm-thick AlN wafer and a 0.5 mm-thick silicon wafer. The resistance of the serpentine heater is about 100 ohms at room temperature. The AlN wafer is used to electrically insulate the silicon wafer. The Ruthenium oxide serpentine heater was printed in AlN wafer surface by the method of printed circuit. To minimize the thermal resistance between the AlN wafer and silicon wafer, a 0.05 mm-thick indium foil (81.6 W/mK, melting point 156 °C) was utilized. The combination was put in an oven at 170 °C for 30 minutes, during which the components stuck together tightly and indium foil's thickness reduced to 0.01 mm due to melting and resolidification. The top cover and the bottom base, the flat silicon heater, and the schematic of narrow channel and the test section are shown in Figures 2, 3 and 4, respectively.

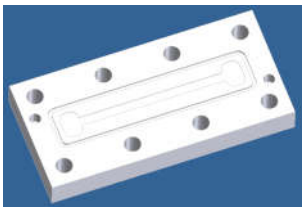

(a) top cover

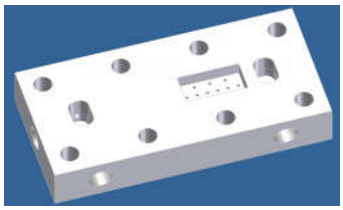

(b) bottom base

(c) Front view

Figure 2. Cover and House for the micro/mini-channel test section

(a) Heater side

(b) Fluid side

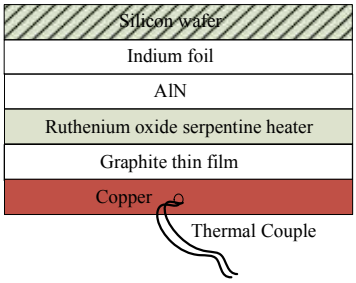

(c) Cross-section of the silicon heater

Figure 3. Silicon heater made of Ruthenium oxide serpentine heater, AlN wafer and silicon

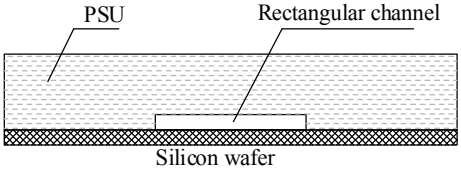

(a) top cover

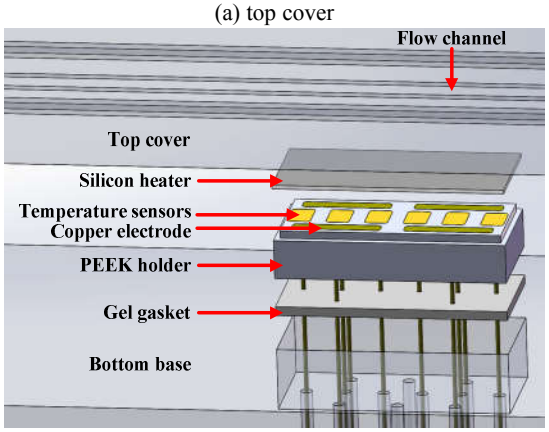

(b) test section assembly

Figure 4. Schematic of micro/mini-gap test section

Surface Characteristics

The silicon wafer used in the subcooled flow boiling experiments was processed by PECVD(Plasma Enhanced Chemical Vapor Deposition), and its surface was covered with one layer of 1 μm-thick silicon dioxide thin film. Figure 5a shows the front SEM image of the silicon wafer. The silicon wafer's silicon dioxide thin film layer was very smooth with nano-sized roughness. Figure 5b shows the side SEM image of the silicon wafer, and the 1 μm-thick silicon dioxide layer can be seen.

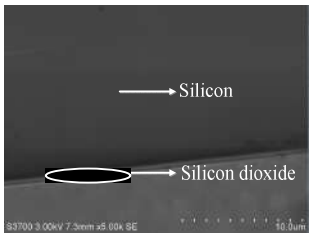

(b) Side

Figure 5. SEM pictures of silicon wafer oxidized by PECVD method

The static contact angle of the surface was measured by the OCA20, DataPhysics Instruments GmbH. As showed in Figure 6, the static contact angle of the silicon dioxide thin film's surface is about 50 ± 3°.

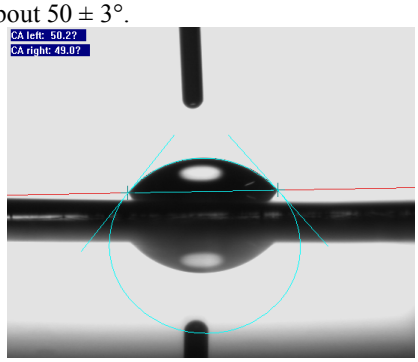

Figure 6. Contact angle pictures of silicon wafer oxidized by PECVD method

Experimental conditions

The experimental mass fluxes ranged from 200 kg/m^{2}s to 400 kg/m^{2}s, the heat flux ranged from 20 kW/m^2 to 300 kW/m^2, the entrance temperature was 90 °C, and the entrance gauge pressure was 10 kPa. The wall temperature was kept below 130 °C to protect the test section. The Phantom high speed camera worked at 1000 fps to visualize the flow patterns of the subcooled flow boiling.

Data reduction

The thermal boundary condition of the test section was assumed to be the uniform axial heat flux and uniform circumferential wall temperature in the bottom of the microchannel with the other sides adiabatic. The heater temperatures were measured at six axial positions, 2.5, 7.5, 12.5, 17.5, 22.5 and 27.5mm from the entrance along the flow direction utilizing six T-type thermocouples. The silicon wafer wall temperatures were calculated through one-dimension heat conduction and the bulk fluid temperatures were given by linear interpolation of the inlet and outlet column temperatures.

For the subcooled flow boiling heat transfer, the effective heat exchange rate between the silicon wafer surface and the fluid can be expressed as:

$$Q_{\text{eff}} = mc_{\text{p}}(T_{\text{out}} - T_{\text{in}}) \quad (1)$$

where Q_{eff}, m, c_{p}, T_{out}, T_{in} are effective heat exchange rate, mass flow rate, the specific heat, outlet temperature and inlet temperature, respectively.

The heat loss of the test section can be calculated as:

$$Q_{\text{loss}} = U \times I - mc_{\text{p}}(T_{\text{out}} - T_{\text{in}}) \quad (2)$$

where Q_{loss}, U and I are the heat loss rate, the voltage and current supplied to the heater in test section, respectively. The heat loss is less than 3% for the single phase and subcooled flow boiling experiments in the constant temperature air bath.

The subcooled flow boiling local heat transfer coefficients are calculated by the equation below:

$$h_{\text{z}} = \frac{q}{\left(T_{\text{w,z}} - T_{\text{f,z}}\right)} \quad (3)$$

where h_z, q, $T_{\text{w,z}}$, $T_{\text{f,z}}$ are local heat transfer coefficient, heat flux, the temperature of silicon surface and fluid at location z in the axial direction, respectively.

The average wall superheat degree of subcooled flow boiling in the microchannel is:

$$\Delta T_{\text{sat, avg}} = T_{\text{w, avg}} - T_{\text{sat, avg}} \quad (4)$$

where $T_{\text{w,avg}}$, $T_{\text{sat,avg}}$ are the arithmetic mean value of the local wall temperature and the local saturation temperature, respectively.

The fluid thermal properties involved in the calculations are based on the local or average bulk temperatures of the fluid.

Experimental uncertainty

Uncertainty of measured parameters and calculated parameters are shown in Table 1.

Table 1 Uncertainty estimation for primary measurements and dependent quantities

Measured parameters	
Channel height and width	±0.005 mm
Test section length	±0.01 mm
Wall and fluid temperature	±0.2 K
Inlet pressure, range: 0-100 kPa	±3.75%
Inlet and outlet differential pressure	±1.5%
Mass flow rate, range: 0 -1.8 g/s	±0.3%
Calculated parameters	
Hydraulic diameter D_{h}, mm	±0.08 mm
Heat flux density q, kW m^{-2}	±3.2%
Vapor quality x	± 0.003
Flow boiling heat transfer coefficient h, W m^{-2} K^{-1}	±12.1%

RESULTS AND DISCUSSION

Subcooled Boiling Curve

Figure 7 shows the subcooled boiling curves at the six axial locations with the mass flux of 400, 300, 200 kg/m^{2}s. At relatively low heat fluxes, the temperatures at the six axial locations increase successively, presenting as single-phase convection heat transfer. At larger heat fluxes, the heat transfer mode changes from the single-phase convection to subcooled flow boiling, with the slope of the boiling curves increasing gradually.

At the onset of nucleate boiling, no nucleate boiling hysteresis behavior was observed. Firstly, the relatively high effective superheat in the thermal boundary layer results in easier nucleation of the bubbles[11]. Secondly, the contact angle between deionized water and the silicon wafer is 50 ± 3°, which is advantageous for bubble generation[12] compared to high-wettability fluids such as FC-72[13-15]. The aspect ratio of the rectangular microchannel is about 10, resulting in lower heat flux for the heated surface near side walls. Along with the thermal conductivity of the liquid is nearly constant, it can be concluded that the temperature gradient (q = - k·∇T) near the side walls is lower. Because of the generally uniform circumferential temperature distribution of the silicon wafer, the effective superheat of the heated surface near side walls is larger, thus it is easier for bubbles to nucleate compared to those near the axis.

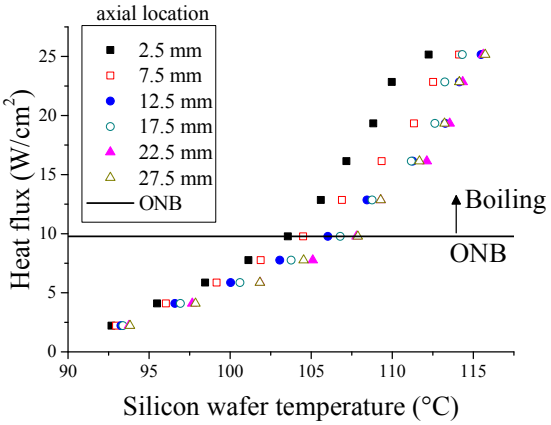

(a)400 kg/m^{2}s

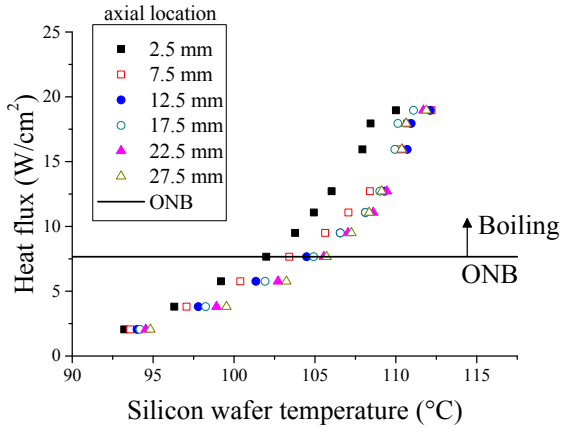

(b)300 kg/m^{2}s

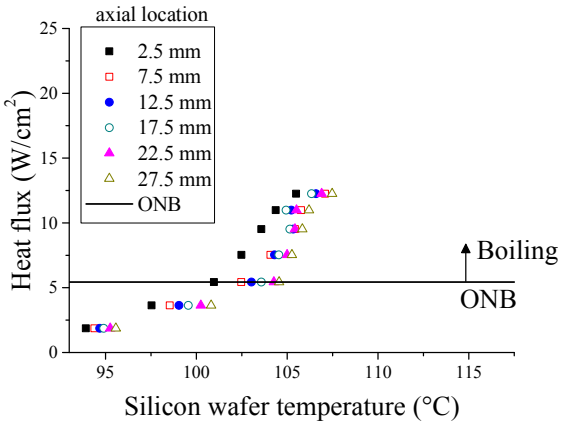

(c)200 kg/m²s

Figure 7. Subcooled boiling curves under different mass fluxes

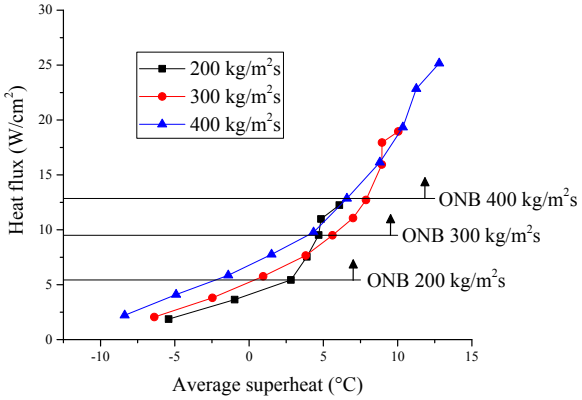

Figure 8. Subcooled boiling curves based on average superheat

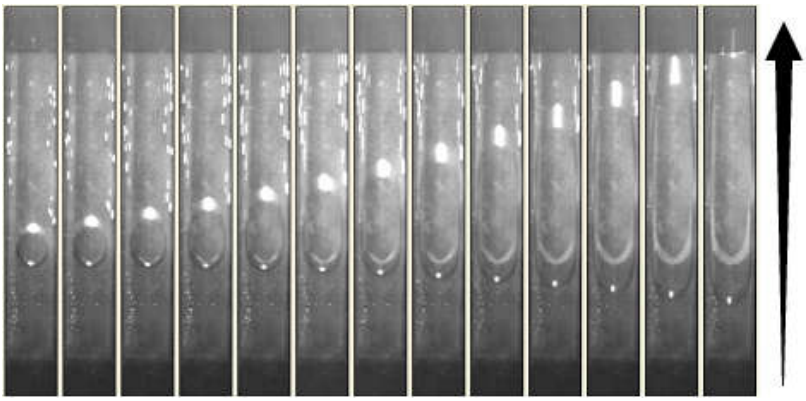

Figure 9. The growth of single bubble to elongated bubble, 200 kg/m²s, 10 W/cm², 1 ms interval

Figure 8 shows the boiling curves based on the average superheat. When the superheat is relatively small, the heat transfer mode is single phase convection. The heat transfer coefficient increases with increased mass flux. The slope of the boiling curves increases sharply when ONB occurs, and the slope is larger for lower mass fluxes with lower superheat needed, because the fluid temperature gradient near side walls is relatively small when the flow velocity is low [11]. At higher superheat degree, transient local dryout phenomenon occurs, leading to smaller slope.

In relatively small mass flux, the size of bubbles is larger and the bubbles are harder to depart from the surface; thus they coalesce with each other, resulting in elongated bubbly flow, as shown in Figure 9. The elongated bubbly flow induces more thin film evaporation, in which transient local dryout and rewet occur frequently, as shown in Figure 10. At smaller heat fluxes, the thin film evaporation is very effective[16]. The alternate between isolated bubbles and elongated bubbles is more frequent with increasing heat flux.

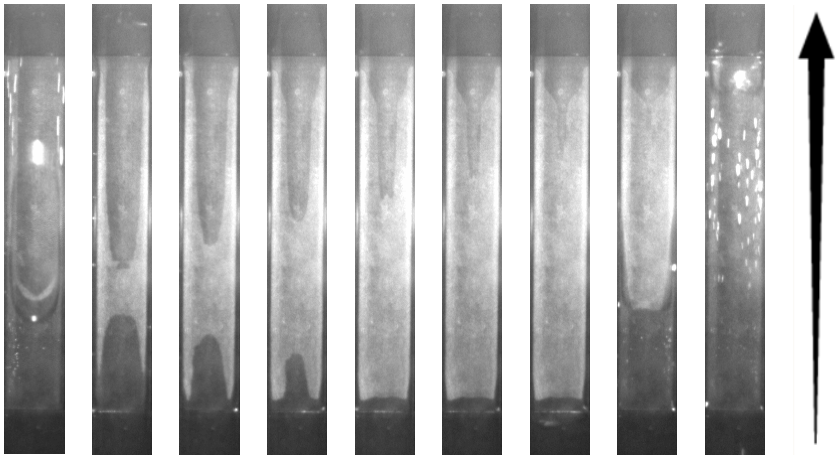

Figure 10. Partial dry-out and rewetting process induced by elongated bubble, 200 kg/m^{2}s, 10 W/cm^2

Heat Transfer Coefficient

Figure 11 (a) - (c) shows the change of the local convective heat transfer coefficients at the six axial locations of the silicon wafer with increasing heat flux at mass fluxes of 400 kg/m^{2}s. 300 kg/m^{2}s, and 200 kg/m^{2}s, respectively. At relatively low heat flux ($q_{eff} < q_{ONB}$), single phase heat transfer dominates the entire test section. The laminar thermal boundary layer thickens gradually along the axial direction, resulting in decreasing local heat transfer coefficient. With the increase of heat flux, the surface of the silicon wafer near exit starts boiling firstly, with sharply increasing heat transfer coefficient. For instance, the heat transfer coefficients at the three downstream locations (h4, h5, h6) of the silicon wafer increase much faster than those at the three upstream locations (h1, h2, h3) at mass flux of 300 kg/m^{2}s. The heat transfer coefficient of the sixth location (h6) increases 1.8 times compared to the single phase heat transfer, while the heat transfer coefficient of the first location (h1) increases 0.6 time only.

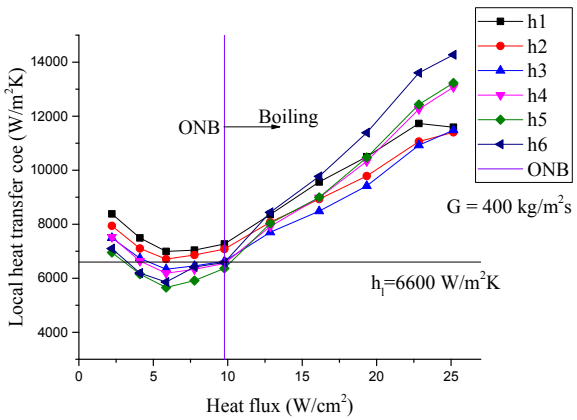

(a) 400 kg/m^{2}s

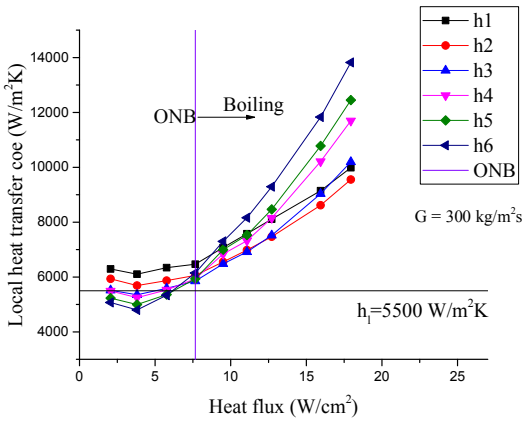

(b) 300 kg/m^{2}s

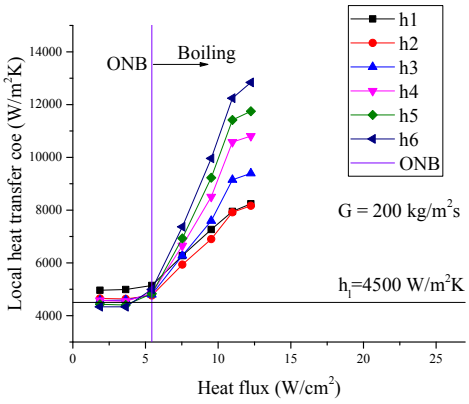

(c) 200 kg/m^{2}s

Figure 11. The variation of local heat transfer coefficients with heat fluxes under different mass fluxes

According to the classic boiling heat transfer theories, flow boiling heat transfer consists of the convective heat transfer and nucleate boiling. The convective heat transfer will be enhanced when the bubbles depart from the heated surface

forming bubbly flow in the microchannel. From the high-speed visualization it can be seen that the bubbles at the entrance of the silicon wafer almost nucleate and grow at the same location, while the bubble departure frequency is low. Meanwhile more vigorous bubbly flow is formed at the downstream surface of the silicon wafer, which has a greater flow disturbance resulting in stronger convective heat transfer. As the fluid subcooling degree at entrance of the silicon wafer is highest along the channel, the effect which suppresses the nucleate boiling is most prominent. Summing up the above two effects, the two-phase heat transfer coefficient downstream of the silicon wafer is much larger than that at the entrance.

CONCLUSIONS

In the present study the ONB of subcooled flow boiling, local heat transfer coefficient, and flow pattern were measured and visualized when deionized water was used as the working fluid in a one-sided heating microchannel with large width-height-ratio and small length-radius-ratio. The fluid inlet temperature was 90 °C, the outlet temperature was lower than the saturation temperature, the mass flux was in the range of 200-400 kg/m^{2}s, and the highest heat flux was 25 W/cm^2.

(1) The heat transfer mode is single phase convection at relatively low superheat. The slope of the boiling curves increases sharply when ONB occurs, and the slope is larger for lower mass fluxes with lower superheat needed.

(2) The flow pattern was mainly isolated bubbly flow when the narrow microchannel was placed vertically. The bubbles generated were larger and not easy to depart at lower mass fluxes, forming elongated bubbly flow and flowing upstream. The thin film evaporation mechanism dominated the entire test section due to the elongated bubbles and transient local dryout as well as rewet.

(3) The local heat transfer coefficient near the exit of the test section was larger. On one hand, the larger number of bubbles and faster bubbly flow velocity downstream made a stronger disturbance to the flow. On the other hand, relatively lower degree of subcooling downstream causes a lower reduction of the nucleate boiling heat transfer.

NOMENCLATURE

A	Flow area, [m^2]
c_p	Constant-pressure specific heat, [J/(kg·K)]
G	Mass velocity, [kg/m^{2}s]
h	Heat transfer coefficient, [W/m^{2}K]
I	Current, [A]
L	Length, [m]
m	Mass flux, [kg/s]
Nu	Nusselt number [-]
P	Pressure, [Pa]
q	Heat flux, [W/m^2]
Q	Heat, [W]
T	Temperature, [K]
U	Voltage, [V]
Greek symbols	
ΔT	Temperature difference, [K]
ΔP	Pressure drop between inlet and outlet, [Pa]
Subscripts	
eff	Effective
f	Fluid
i	Local
l	Liquid
loss	Heat loss
ONB	Onset of nucleate boiling
sat	Saturation
w	Wall
z	Axis direction

ACKNOWLEDGMENTS

This work is supported by the PhD Program Foundation of Ministry of Education of China (20120101110102), National Science Foundation of China (51210011), National Science Foundation of Zhejiang Province (LZ13E060001) and the MISTI Greater China Fund for Innovation. The authors thank Professor Shu-Shen Lu at Sun Yat-Sen University for providing the graphite sheet.

REFERENCES

[1] WANG P, MCCLUSKEY P, BAR-COHEN A. Two-phase liquid cooling for thermal management of IGBT power electronic module [J]. Journal of Electronic Packaging, 2013. 135(2): 021001.

[2] TUCKERMAN D B, PEASE R. High-performance heat sinking for VLSI [J]. Electron Device Letters, IEEE, 1981. 2(5): 126-129.

[3] KANDLIKAR S G. History, advances, and challenges in liquid flow and flow boiling heat transfer in microchannels: A critical review [J]. Journal of Heat Transfer, 2012. 134(3): 034001.

[4] LI W, WU Z. A general correlation for evaporative heat transfer in micro/mini-channels [J]. International Journal of Heat and Mass Transfer, 2010. 53(9-10): 1778-1787.

[5] LI W, WU Z. A general criterion for evaporative heat transfer in micro/mini-channels [J]. International Journal of Heat and Mass Transfer, 2010. 53(9-10): 1967-1976.

[6] ALAM T, LEE P S, YAP C R et al. A comparative study of flow boiling heat transfer and pressure drop characteristics in microgap and microchannel heat sink and an evaluation of microgap heat sink for hotspot mitigation [J]. International Journal of Heat and Mass Transfer, 2013. 58(1-2): 335-347.

[7] BAR-COHEN A, SHEEHAN J R, RAHIM E. Two-phase thermal transport in microgap channels—theory, experimental results, and predictive relations [J]. Microgravity Science and Technology, 2012. 24(1): 1-15.

[8] KOTTKE P, YUN T M, GREEN C E et al. Two phase convective cooling for ultra-high power dissipation in microprocessors. In Thermal and Thermomechanical Phenomena in Electronic Systems (ITherm), 2014 IEEE Intersociety Conference on. 2014: IEEE.

[9] SHOJAEIAN M, KOŞAR A. Pool boiling and flow boiling on micro- and nanostructured surfaces [J]. Experimental Thermal and Fluid Science, 2015. 63: 45-73.

[10] BHAVNANI S, NARAYANAN V, QU W et al. Boiling augmentation with Micro/Nanostructured surfaces: Current status and research outlook [J]. Nanoscale and Microscale Thermophysical Engineering, 2014. 18(3): 197-222.

[11] COLLIER J G, THOME J R. Convective boiling and condensation [M]. Oxford University Press, 1994.

[12] PHAN H T, CANEY N, MARTY P et al. Flow boiling of water on nanocoated surfaces in a microchannel [J]. arXiv preprint arXiv:1008.4696, 2010.

[13] CHANG W R, CHEN C A, KE J H et al. Subcooled flow boiling heat transfer and associated bubble characteristics of FC-72 on a heated micro-pin-finned silicon chip [J]. International Journal of Heat and Mass Transfer, 2010. 53(23–24): 5605-5621.

[14] SITAR A, SEDMAK I, GOLOBIC I. Boiling of water and FC-72 in microchannels enhanced with novel features [J]. International Journal of Heat and Mass Transfer, 2012. 55(23-24): 6446-6457.

[15] SHIN S, CHOI G, KIM B S et al. Flow boiling heat transfer on nanowire-coated surfaces with highly wetting liquid [J]. Energy, 2014. 76(0): 428-435.

[16] THOME J R. Boiling in microchannels: A review of experiment and theory [J]. International Journal of Heat and Fluid Flow, 2004. 25(2): 128-139.